Prediction of Brinell Hardness Distribution in Cold Formed Parts

Ahmet Demir

Fazil O. Sonmez[1]

Department of Mechanical Engineering,
Bogazici University,
Istanbul, Bebek, 34342, Turkey

The objective of this study is to predict the Brinell hardness distribution in cold formed parts by relating the plastic strains found by finite element (FE) analysis to hardness. Based on the material's plastic flow curve, an analytical relation was established between the plastic strain induced in the metal during cold working and its Brinell hardness so that its hardness can be determined from numerically obtained plastic strains without producing the part and taking measurements. In order to verify the model developed in this study, cold extrusion experiments were performed on samples made of two different metals at five different extrusion ratios. These samples were cut, and at their centers Brinell hardness measurements were taken, which were then compared with the analytical predictions. The results of the analytical model compared quite well with the data obtained from experiments. The model was also verified by comparing its predictions with the experimentally determined values of hardness reported by previous researchers. The results showed that within the applicable range of Brinell hardness test, which covers a great percentage of hardness levels resulting from cold forming operations, the analytical model can reliably be used. [DOI: 10.1115/1.1789960]

Keywords: Brinell Hardness, Flow Curve, Effective Strain, Spherical Indentation, Cold Forming, Extrusion, Plastic Deformation, Steels

Introduction

If a volume of metal is cold worked, the resulting plastic strain distribution may not be uniform. Knowing that inducing plastic deformation alters material's strength, different regions of a cold formed part will have different strength. For part reliability, we need to characterize and determine its strength. A practical way of characterizing strength is hardness.

Hardness as a measure of material's resistance to permanent deformation is an important quality parameter for the finished product. It is also a measure of forgeability of a material undergoing a cold forming process. Generally, cold-formed parts are forged in a number of stages and in each stage the material undergoes additional permanent deformation. The material, during the process, sometimes becomes so hard that further forming becomes impossible without fracturing the part. In order to continue the process, the part should be heat treated, and thus its hardness should be reduced. Therefore, it is important to know whether all stages can be achieved consecutively without any interruption of forming process or a heat treatment is necessary at some intermediate stage.

Because of being an important quality criterion, a measure of strength, and a means of determining formability of the material, we need to determine the hardness of a part. Trial and error, by producing prototypes, taking measurements and repeating the process, is not a feasible approach. It is difficult, time consuming, and costly. Estimating the hardness distribution without actually making the part is a more desirable approach.

In order to establish a correlation between effective strain and hardness, Kim, Lee, and Altan [1] performed an upsetting experiment, and then measured the hardness at various locations in the part. They also calculated effective strain distribution in the upset part through a FE analysis of the upsetting process. By correlating the measured hardness and the numerical results, they found a relation between Vickers hardness and effective strain. They also checked the validity of this relation by comparing numerically determined effective strain distribution in a backward extruded can to the measured hardness distribution. Gouveia et al. [2,3] performed a similar study for cold forward extrusion. They obtained a relation between Vickers hardness and effective strain by measuring the hardness at the center of cylindrical specimens compressed at specific ratios. According to the compression ratio, the compressed specimens had known values of effective strain. They used their relation to verify the numerically calculated effective strain distribution in an extruded part by comparing with the measured hardness distribution. Ruminski et al. [4] obtained an empirical relation between Vickers hardness and effective strain to determine the mechanical property distribution in cold drawn tubes. However, these were empirical relations specific to certain materials with a certain flow curve. If one seeks a relation between hardness and strain for another material, an upsetting test, hardness measurements, and FE simulations are required followed by correlation with results. Choi et al. [5] avoided this burdensome procedure by performing a FE simulation of the Brinell hardness test for a cold formed material. Thus, they obtained Brinell hardness of a material that has undergone a certain extent of plastic strain. Based on the calculated hardness they found a relation between hardness and strain, and then verified this relation by comparing the predicted hardness distribution with the measured values. Although they avoided the cumbersome experimental work that the previous methods required, their approach still poses difficulties concerning accurate FE modeling of the Brinell test indentation, and computational expense of such a nonlinear contact problem with moving contact boundaries. Similarly, Tekkaya [6] carried out a FE analysis of conical indentation on a cold worked part to find the equivalent pyramidal Vickers hardness and obtained a relation between Vickers hardness and flow stress.

In this study, we propose an analytical relation between the Brinell hardness of a cold formed material and the effective strain based on the flow curve constants of the unformed material. Accordingly, we avoid formidable experimental and numerical procedures.

[1]Author to whom correspondence should be addressed. Tel: +90 212 359 7196; Fax: 90 212 287 2456; e-mail: sonmezfa@boun.edu.tr

Contributed by the Materials Division for publication in the JOURNAL OF ENGINEERING MATERIALS AND TECHNOLOGY. Manuscript received by the Materials Division July 31, 2003; revision received April 5, 2004. Associate Editor: A. M. Rajendran.

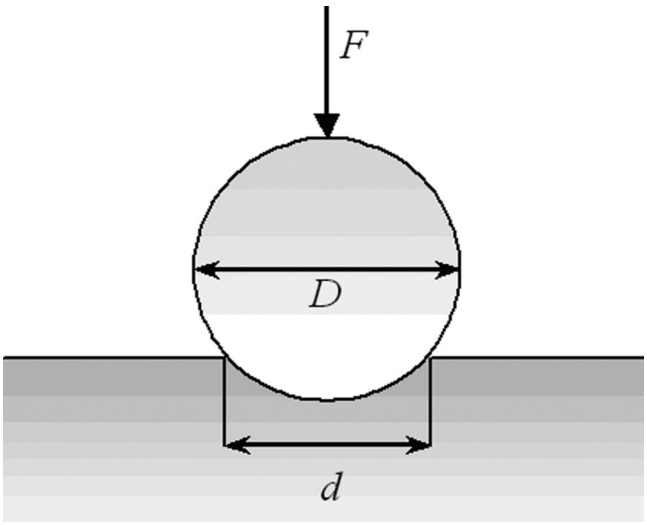

Fig. 1 A schematic for the spherical indentation of the Brinell hardness test

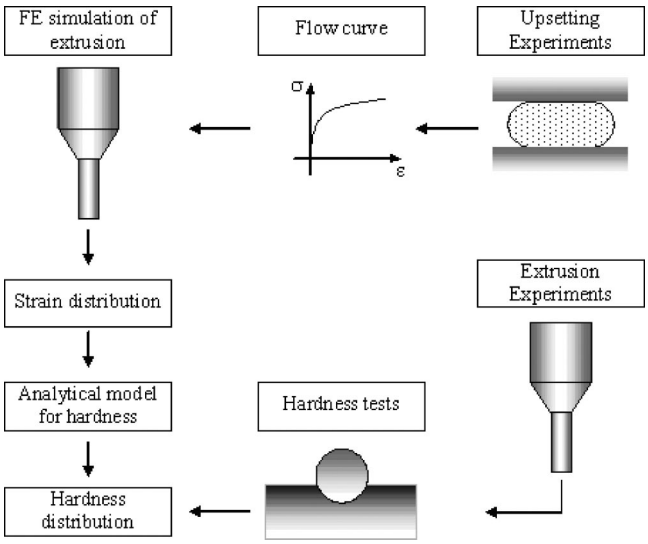

Fig. 2 Schematic of the procedure for verifying the analytical model

Approach to the Problem

The Brinell hardness test (Fig. 1) is performed by forcing a hardened steel (or tungsten carbide) ball with diameter D onto the part being tested with a specified force, F, and measuring, by a magnifier or microscope, the diameter of the indented area, d. The Brinell hardness, HB, is defined as the load per unit surface area of the permanent impression:

$$\mathrm{HB}=\frac{F/D^2}{\frac{\pi}{2}\left(1-\sqrt{1-\left(\frac{d}{D}\right)^2}\right)} \tag{1}$$

here F is in kgf, D and d are in mm. Accordingly, the unit of HB is kgf/mm^2. For steels having hardness less than 650 HB, the standard value of the F/D^2 ratio is 30 kgf/mm^2. Usually, the chosen values for F and D are 3000 kgf and 10 mm [7]. Hence, having measured or estimated the indentation diameter, d, one may easily calculate HB.

We may assume that the deformation behavior of the material fits a simple power law such that if the material is under uniaxial loading, the true stress-true strain curve can be described by

$$\sigma=\kappa\varepsilon^n \tag{2}$$

where κ and n are material constants. The strain hardening exponent, n, ranges from 0.0 (zero work hardening) to an upper limit of about 0.5 [8]. In this study, we analytically related the indentation diameter, d, and Brinell hardness, to the flow curve constants κ and n. We relied on the previous theoretical and empirical studies of the Brinell indentation process. We also generalized this relation to the cases where the material has undergone permanent deformation through cold forming.

Figure 2 describes the procedure that we followed to verify the analytical model. First, two different materials were selected and their flow curves were determined through upsetting (compression) experiments. Effective strain at the central line of the extruded parts away from the edges was already known analytically. Besides, FE analysis of the extrusion process was carried out to find the effective strain distribution. Thus, it was possible to ascertain the region where analytically calculated strains were valid. Then, the hardness corresponding to the effective strains was predicted through the analytical model. The results were then compared with the measured hardness. The analytical model was also verified by checking how well it predicts the experimental results reported by the previous researchers.

The Analytical Model to Predict Brinell Hardness

The mechanical behavior of an indented solid can be characterized as purely elastic, elastoplastic, or fully plastic. If the indentation force is small, the material elastically deforms and upon unloading the surface recovers to its original shape. A further increase in the load leads to plastic deformation, initially half contact radius below the surface, where maximum shear stress develops [9]. If the load is further increased, the plastic region extends, during which resistance of the material against deformation increases due to work hardening. Continued indentation thus requires larger and larger mean pressure. Beyond the elastic-plastic regime, a fully plastic regime follows, in which plastic zone extends over the whole region around the indentation. Hardness measurements are carried out in the fully plastic regime; hence correlation of experimental and analytical results should be done for this regime.

In 1908 Meyer developed an empirical relation [10] such that the ratio of indentation diameter to the ball diameter, d/D, increased with the mean pressure, P_m, as

$$P_m=k\left(\frac{d}{D}\right)^m \tag{3}$$

where, P_m is the load per unit projected area

$$P_m=\frac{F}{\pi d^2/4} \tag{4}$$

The data provided by O'Neill in 1944 [10,11] suggested that the power m in Eq. (3) was about equal to the strain hardening exponent, n, in Eq. (2). Further experimental studies confirmed this finding [12,13].

Based on indentation tests performed on highly worked materials Tabor [8,11] found that mean pressure, P_m, was about equal to $3\sigma_e$, flow stress, in the fully plastic regime regardless of the indentation size. Because they were incapable of further appreciable work hardening, they can be considered to be ideally plastic material. Accordingly, flow stress, σ_e, can be assumed to be uniform around the indented region. On the other hand, when a work hardening material is indented by a spherical indenter, the flow stress (or yield stress, S_y) increases as a result of the strain hardening of the material. We should recognize that the extent of deformation, or strain (ε), changes from one point to another in the indented region, so does the flow (or yield) stress according to Eq. (2). This means that for work hardening materials, flow stress not

only varies with deeper penetration but also varies spatially in the indented region. Tabor [11] assumed that at a material point developed a flow stress, σ_e, that could be considered to be representative of the overall deformation. He further assumed that the representative stress had a linear relation with the average pressure.

$$P_m = \alpha \sigma_e \tag{5}$$

where α is a constant. At this material point, the representative stress, σ_e, and strain, ε_e, are also related according to Eq. (2).

$$\sigma_e = \kappa \varepsilon_e^n \tag{6}$$

Tabor, reasoning from the equality of strain distributions for indentations at which d/D ratio is the same because of the same deformed shape, concluded that the representative strain would also depend on this ratio. In order to find the point of representative flow stress, Tabor first established a relation between pyramidal Vickers hardness and the flow stress of the material based on measured values of hardness on specimens compressed by specific ratios, therefore with known flow stress. Then, he conducted micro pyramidal indentations on the surface of spherical indentations, and thus determined the flow stress of the deformed material at various locations on the free surface. Based on the data, he found out that the flow stress at the edge of the indentation was proportional the mean pressure, P_m, over a wide range of indentation sizes (d/D) such that Eq. (5) holds with a value of α approximately equal to 2.8 (for various materials, it was between 2.6 and 3.0). Accordingly, he supposed that it might be used as a representative value for the overall deformation of the material around the impression. The corresponding representative strain at the edge found from Eq. (6) turned out to be related to the d/D ratio (confirming Eq. (3) and equality of n and m) as

$$\varepsilon_e = \beta \frac{d}{D} \tag{7}$$

here, β was about equal to 0.2 independent of n or κ. Substituting Eqs. (3), (6), and (7) into Eq. (5), we obtain

$$\frac{F}{\pi d^2/4} = \alpha \kappa \left(\beta \frac{d}{D} \right)^n \tag{8}$$

The ratio of mean pressure P_m, to yield stress S_y, at the onset of permanent deformation during indentation takes a value of about 1.1 [9,14,15]. In order to induce a deeper indentation, this ratio needs to be increased, but when the ratio becomes equal to α in the fully plastic regime, in which hardness measurements are taken, it remains constant [11]. Taking out the indentation diameter, d, in Eq. (8), we get

$$d = \left(\frac{4FD^n}{\pi \alpha \kappa \beta^n} \right)^{1/(n+2)} \tag{9}$$

Substituting for d in Eq. (1), and rearranging, we may express the Brinell hardness, HB, in terms of the known properties.

$$\mathrm{HB} = \frac{F/D^2}{\frac{\pi}{2}\left(1 - \sqrt{1 - \left(\frac{4}{\pi \alpha \kappa \beta^n} \frac{F}{D^2} \right)^{2/(n+2)}} \right)} \tag{10}$$

Equation (10) implies that as long as the F/D^2 ratio remains constant (the standard is 30 kgf/mm^2 for steels), the same Brinell hardness is obtained for a given material regardless of the applied force, F. Having determined flow curve constants (κ and n), we can easily calculate the Brinell hardness.

In a cold forging process, plastic strains are induced, and consequently hardness of the work-piece increases due to strain hardening. Equation (10), however, does not account for the effect of work hardening. Therefore, it is valid only for materials with no prior deformation. Tabor confirmed that initial uniaxial strain, ε_o, is additive to the representative strain, ε_e. Equation (7) then becomes

$$\varepsilon_e = \varepsilon_o + \beta \frac{d}{D} \tag{11}$$

Substituting Eqs. (6) and (11) into Eq. (5), we may express the average pressure as

$$\frac{F}{\pi d^2/4} = \alpha \kappa \left(\varepsilon_o + \beta \frac{d}{D} \right)^n \tag{12}$$

Equation (12) may not be solved for d analytically. We need to employ numerical methods. After substituting the numerically obtained value for d in Eq. (1), we may easily calculate HB.

Ruminski et al. [4] found that compression and tension specimens deformed to the same level of effective strain possessed about the same hardness. This fact justifies our assumption made in deriving Eq. (12) that hardness of a material is uniquely related to the level of effective strain regardless of the deformation history. However, for materials for which tension and compression flow curves are highly discrepant such as austenitic stainless steels [6] Eq. (12) will not be valid.

Effective Strain

During forging of intricate parts, unlike uniaxial loading, deformation state becomes very complex. At a material point, all of the strain components, ε_{ij}, may be nonzero. However, in order to be able to employ Eq. (11) we need a single strain, ε_o, that is representative of the prior deformation at that point. In this study, we assume that Eq. (11) as well as Eq. (12) are valid if effective strain is used for ε_o. According to the deformation theory of plasticity, effective strain is defined as

$$\varepsilon_o = \sqrt{\tfrac{2}{3}(e_{11}^2 + e_{22}^2 + e_{33}^2 + 2e_{12}^2 + 2e_{13}^2 + 2e_{23}^2)} \tag{13}$$

As can be seen, in uniaxial loading of an incompressible material ($\nu = 1/2$), where only σ_{11} is nonzero, effective strain reduces to ε_{11}. For further information, one may refer to books on plasticity like Ref. [16].

The Factors α and β

Tabor [11] experimentally determined the values of α and β in Eq. (8) as 2.8 and 0.2. Researches investigated through empirical, theoretical and numerical studies whether these values were just empirical fit obtained by just averaging the data on a few chosen materials, or they possessed a general validity. Most of these researchers confirmed the form of Eq. (8), but differed on their choice of appropriate values for α and β. Richmond, Morrison, and Devenpeck [17] obtained a theoretical solution for the indentation of a rigid-perfectly plastic solid by a rigid sphere. The theory predicted that the ratio of the mean pressure to yield stress (α) was 3.0, and this value remained constant throughout penetration, and the representative strain of the deformed material was approximately equal to 0.32 (β) times the impression-to-ball-diameter ratio. However, indentation experiments on a copper alloy showed that the theory somewhat overestimated these values. Follansbee, Sinclair, and Johnson [14,18] performed a FE elastoplastic analysis of a work-hardening material indented by a rigid ball. Their results agreed with the experimental data provided by Tabor [11] in the elastoplastic as well as in the fully plastic regime. Some other FE studies of spherical indentation [19,20] also corroborated Tabor's findings. Hill et al. [21] analyzed the Brinell indentation on power-law hardening materials using the deformation theory of plasticity. They formulated the problem using a self-similarity approach such that deformed geometry, stress and strain fields could be derived from a single stationary solution by appropriate scaling. Path (or history) dependence was thus removed. They obtained a solution of the problem by a finite ele-

Table 1 Measured and calculated (Eq. (10)) hardness values of materials with no initial strain

Material (Steel)	κ (MPa)	n	Measured HB	Predicted HB	%Error
AISI1010 [1]	665	0.255	98*	99	1.7
WNr. 1.0303 [2,3]	685.2	0.185	110*	119	8.4
XC18 [28]	664	0.10	142*	140	1.1
SCM415 [5]	768	0.139	143	149	4.0
Z2CN18-10 [28]	862	0.21	148*	142	4.3
Mild steel [11]	1000	0.249	149*	150	0.7
XC80 [28]	921	0.17	159*	166	4.1
35CD4 [28]	819	0.09	185*	178	3.7
XC48 [28]	1133	0.16	195*	208	6.5
16NC6 [28]	1026	0.17	196*	184	6.1
100C6 [28]	1023	0.14	196*	197	0.6
42CD4 [28]	939	0.10	204*	200	2.2
Z38CDV5 [28]	1136	0.17	213*	203	4.6
XC38 [28]	1102	0.11	221*	228	3.5
XC65 [28]	1607	0.24	221*	239	8.3
0.3C, 0.4Mo, 1.4Mo,1.6Ni temp. at 725°C [12]	1137	0.120	247*	230	7.0
ASTM A514, T1 [30]	1103	0.088	256	242	5.6
A508B [29]	1133	0.105	258*	238	7.9
35NC15 [28]	1235	0.08	272*	276	1.5
Z15CN17-03 [28]	1403	0.10	288*	297	3.3
AISI 4130 tempered at 670°C [27]	1300	0.096	297*	279	6.3
AISI 4130 tempered at 550°C [27]	1375	0.070	338*	316	6.6
0.3C, 0.4Mo, 1.4Mo, 1.6Ni temp. at 425°C [12]	1534	0.061	402*	361	10.2
AISI 4130 tempered at 400°C [27]	1860	0.049	458*	452	1.3
AISI 4130 tempered at 300°C [27]	2213	0.056	535*	527	1.6
0.3C, 0.4Mo, 1.4Mo, 1.6Ni temp. at 200°C [12]	2163	0.050	537*	524	2.4

*Vickers hardness was converted to Brinell hardness using the conversion table for steels provided in Ref. [31].

ment method. Remarkably, their numerical solution yielded about the same universal values, $\alpha=2.8$, and $\beta=0.2$ in Eq. (8), as the values determined experimentally by Tabor [11]. At the perimeter, the effective strain was found to be $0.2d/D$ regardless of the value of strain hardening exponent. Biwa and Storakers [22] carried out a similar analysis, but used incremental (or flow) theory of plasticity. Their analysis yielded $\alpha=3.07$, and $\beta=0.16$. Estimated effective strain distributions in these two studies were incompatible. In a recent FE study conducted by Mesarovic and Fleck [23], a drop was predicted in the value of α for large indentations in the fully plastic regime. However, this drop occurs beyond the range in which most hardness measurements are taken. Francis [15] carried out a statistical analysis of previously published spherical indentation data. The mean value of α for 21 different materials having a low strain hardening exponent, n, turned to be 2.87. Francis also confirmed the suitability of the form of Eq. (7) using indentation data from 43 materials. Chaudhri [13,24] investigated effective strain distribution around spherical indentations on copper specimens. He first obtained an empirical relation between Vickers (pyramidal) hardness and plastic strain based on the hardness measurements on specimens each having a specific compression ratio. After carrying out a Brinell indentation, he cut the specimen through the mid plane of the impression. He then performed micro Vickers hardness measurements on the cut section and obtained the strain distribution by correlating with the measured hardness. Empirically found strain qualitatively agreed with the calculated strain of Hill et al. [21] in locating the maximum strain just below the indentation surface on the load axis. Yet, the representative strain turned out to be nonlinearly dependent on d/D ratio as opposed to the linear dependence as confirmed by Hill et al. [21] and Francis [15]. Based on this, Chaudhri [24] questioned the validity of Eq. (7). However, the indentations in this study were far larger than the ones on which standard Brinell hardness measurements are taken. Matthews [25] developed a model for indentation, which showed dependence of α on strain hardening exponent, n. For a perfectly plastic material ($n=0.0$) α was 3.0, and $\alpha\simeq 2.85$ for $n=0.5$. A FE analysis of spherical indentation carried out by Taljat et al. [26] suggested the same trend. Tirupataiah and Sundararajan [12,27], assuming $\beta=0.2$, conducted static indentation tests to find the value of α. Relying also on previously reported experimental data, they evaluated the reliability of the indentation models proposed by other researchers. They found none of the models they considered to be satisfactory. For various materials, α came out to be between 2.4 and 3.0. Although the predictions of Matthew's model compared well with the data for steels, over aged Al alloy, and Cu–Zn, the model overestimated the value of α for iron, copper, and Al alloy in aged condition. They suggested that lower strength materials having hardness less than about 200 HB exhibited lower α values. Review of the literature reveals that there are disagreements among researchers regarding the relation between mean pressure and the extent of indentation.

Comparison Between Measured and Predicted Values of Hardness. In order to test the appropriateness of the suggested values for α and β, a comparison is made between the measured hardness of materials with known flow properties and the hardness calculated by the analytical model developed in this study. Because forging of steels is our main emphasis in this study, we only considered steel properties reported in the literature. As seen in Table 1, the flow parameters (κ and n) of the 26 chosen materials have a wide range of values (0.049–0.255 for n, 664–2213 MPa for κ, 98–537 kgf/mm^2 for HB). Because the hardness of these materials was measured before any prior deformation (i.e., work hardening), Eq. (10) was employed using the suggested α and β values. The empirical values ($\alpha=2.8$, and $\beta=0.2$) proposed by Tabor [11], and confirmed by the analyses of Hill et al. [21] and Follansbee, Sinclair, and Johnson [14,18] turned out to be the most appropriate ones in predicting the hardness of a steel material. The average error in HB for the chosen materials is 4.4% with a standard deviation of 2.7, and the maximum error is 10%. There is no need to decrease the value of α for low strength steels as opposed to the suggestion made by Tirupataiah and Sundararajan [12] for iron and copper.

Because our objective was to estimate the Brinell hardness of cold forged products, the validity of the proposed equation in estimating the hardness of permanently deformed materials is of higher importance. In view of this, we compared the predictions of the proposed equation first with the experimental data reported by Kim, Lee, and Altan [1]. In Fig. 3, data points indicate the hardness measured at specific locations in compression specimens corresponding to the numerically calculated effective strains. The

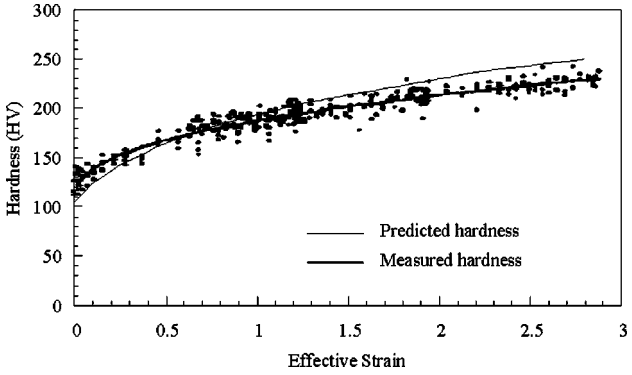

Fig. 3 Data points indicate the measured hardness corresponding to the numerically calculated values of effective strain [1] for AISI 1010. The thicker line shows the empirical curve obtained by curve fitting of the data points. The thinner line shows the hardness predicted by the proposed equation (Eq. (12) together with Eq. (1)).

thicker line shows the empirical curve obtained by curve fitting of the data points ($HV = 102.8 + 84.9\varepsilon_o^{0.4}$) [1]. The thinner line shows the hardness predicted by the proposed equation (Eq. (12) together with Eq. (1)) using the flow parameters of the undeformed material (the Brinell hardness was converted to Vickers hardness using the conversion table in Ref. [31]). Calculated values of hardness are within the range of the data scatter even for very large effective strains. The empirical values ($\alpha = 2.8$, and $\beta = 0.2$) proposed by Tabor [11] again provided the best fit.

Figure 4 provides another comparison between the predicted and measured hardness. The triangular marks show the hardness measured by Gouveia et al. [2,3] at the center of cylindrical specimens compressed at specific ratios, therefore with known values of effective strain. Although, the proposed equation somewhat overestimates the hardness, the predicted trend in hardness with induced deformation agrees with the experimentally determined trend. The maximum error is 14%, and on the average the error is about 11%. Considering the various sources of error, the agreement of the analytical predictions with the empirical data is good.

We further verified the proposed equation by comparing its predictions with the values of hardness measured by Tabor [11] on cylindrical specimens with known effective strain (Fig. 5). The predictions of the model agree quite well with the data.

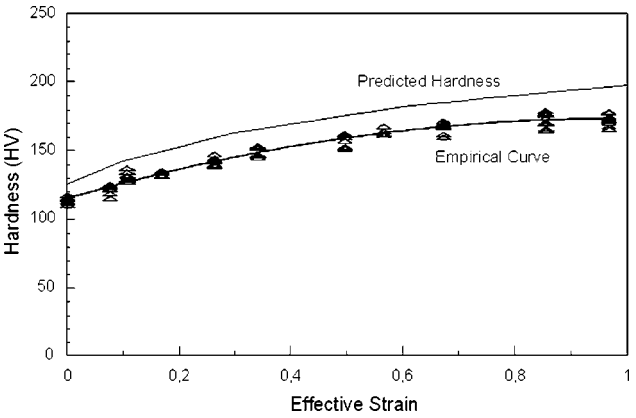

Fig. 4 The thicker line shows the empirical curve obtained by curve fitting of the data points ($HV = -60.7\varepsilon_o^2 + 119.1\varepsilon_o + 115.1$) [2]. The thinner line shows the hardness predicted by the proposed equation (Eq. (12) together with Eq. (1)).

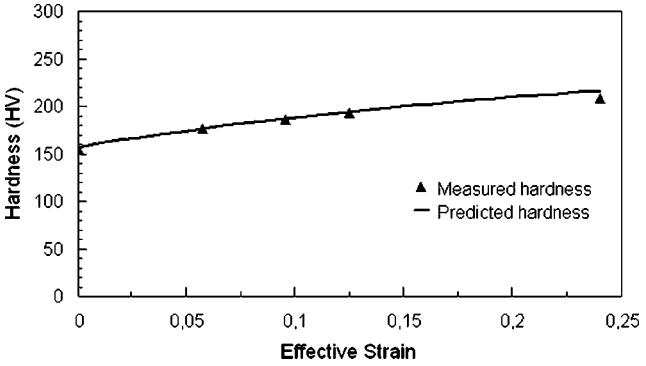

Fig. 5 Data points indicate the measured hardness of a mild steel [11]. The line shows the hardness predicted by the proposed equation (Eq. (12) and Eq. (1)).

Cold Forming Experiments

The experimental part of this study involves validation of the analytical relation between effective strain and the Brinell hardness, and examining applicability of the method developed in this study. As a forming process, cold extrusion was chosen, firstly because it is possible to analytically determine the final plastic strain along the centerline of the extruded part. Thus, the error due to numerical analysis of deformation for determining the value effective strain was avoided. Secondly, one may easily impose any value of strain by just varying the ratio of initial diameter to final diameter. Thirdly, extruded parts are widely used in industrial applications either as a semi or final product. Also, upsetting (open-die forging) experiments were conducted to establish the relation between the true stress and strain.

Material. In cold forming, usually low-carbon steels are used. Accordingly, the selected materials for extrusion were C40 and St37, which had the chemical composition as given in Table 2. Billets were normalized before the cold forming experiments in order to attain a homogenous and relatively soft microstructure. Although any metal or alloy can be extruded, in practice die strength sets a limit for the strength of the material to be extruded. In this study, dies were made of cold worked tool steels, hardened to 60 HRc, which endured through the extrusion process without sustaining any damage.

Table 2 Chemical composition of C40 and St37 steels

Material	C%	Mn%	S%
C40	0.37–0.44	0.5–0.8	<0.045
St37	<0.17	0.2–0.5	0.03

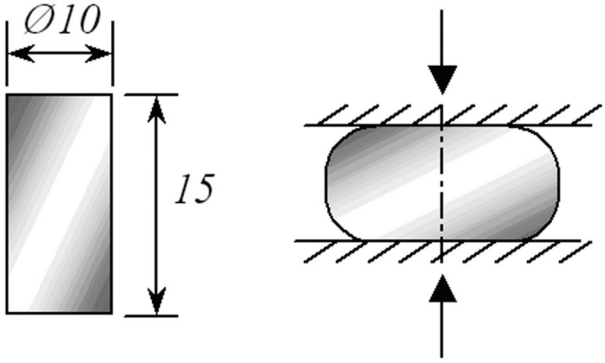

Fig. 6 Upset part dimensions

Table 3 Flow curve constants of C40 and St37 ($\sigma=\kappa\varepsilon^n$)

Material	K (MPa)	n
C40	810	0.150
St37	773	0.171

Upsetting Experiments. First, in order to characterize plastic flow behavior of the materials, i.e., to obtain the flow curve constants, upsetting experiments were carried out. Three samples were made from each material. The samples had a diameter of ∅10 mm and a length of 15 mm as shown in Fig. 6. The experimental procedure for upsetting was standardized in ASTM E9-81. The dimensions of the test-piece and surface finish were selected, and upsetting experiments were performed by following the standard procedure as detailed by Pohland [32]. The test machine provided the force and displacement data, which were then used to construct the true-stress-and-strain curves. Table 3 presents the constants of the flow curves represented by a power relation, $\sigma=\kappa\varepsilon^n$.

Extrusion Experiments

Setup. The basic experimental setup mainly consisted of a die and a punch. All other equipments were accessories to fix these two main parts onto the press table. The final diameter, D_e, was the same for all dies, which was 15 mm; on the other hand, a different initial diameter was chosen for each die. Five different dies and punches were manufactured with different reduction ratios. The dies and the punches were made of hardened tool steels. Figure 7 gives a sketch of the parts for the die-set.

The punch was fixed by means of a punch holder to the upper block, which was in turn fixed to the ram of the press. The punch holder was positioned so as to provide concentricity of the punch and the die. The material of the die was hardened and the surface was ground to reduce friction so that resistance to material flow would be as low as possible. The lower block stood between the press table and the die. The material extruded into the lower block, which had a bore slightly larger than D_e. The half cone angle was 20 deg.

In order to ensure a uniform and homogenous extruded portion, the length of extrusion, h, was chosen to be about four times the outlet diameter, $D_e=15$ mm, or three times the initial diameter.

Table 4 Strains and extrusion ratios of the extruded parts

Part number	Initial diameter D_o (mm)	Extruded diameter D_e (mm)	True strain $2\ln(D_o/D_e)$
1	30,2	15	1,40
2	27,3	15	1,20
3	23,5	15	0,90
4	19.3	15	0,50
5	17,0	15	0,25

The thickness of the head, H, is as large as the inlet diameter, D_o. If the part were extruded further, then a sucking-in would occur (if $H<D_o$) at the head. This means a cavity forms at the top surface of the head as if indented with a sphere, because of more extensive flow at the center.

The Extrusion Ratios. Five extrusion ratios were chosen, which resulted in five different final strain values. Table 4 shows the dimensions of the extruded part, and the associated central strains.

Plastic Strain Distribution in the Extruded Specimens. Although the effective strain at the centerline of the extruded part was analytically determined as $2\ln(D_o/D_e)$, due to edge effects validity of this formula is restricted to portions of centerline away from the edges. In order to investigate the range for which this formula is valid, the extrusion process was modeled using Marc Autoforge to determine the effective strain distribution. One may refer to Ref. [33] for the details of this analysis.

After performing the FE simulations, the centerline strains were observed to be equal to the value $2\ln(D_o/D_e)$ away from the edges. In other words the speed of the punch and the material properties had almost no effect on the final strain at the centerline. The final geometry and the strain distribution are shown in Fig. 8. The head length, x_h, and the initial unstable process region x_e-x_a, roughly equals to the inlet diameter. In order to capture the strain without the effect of free edges the length of the extruded part, x_e-x_t, was chosen to be about three times the initial diameter. Thus, the measurements were taken in the region between x_t and x_a, to make a valid comparison between the analytically predicted and measured values. The strains at other locations can

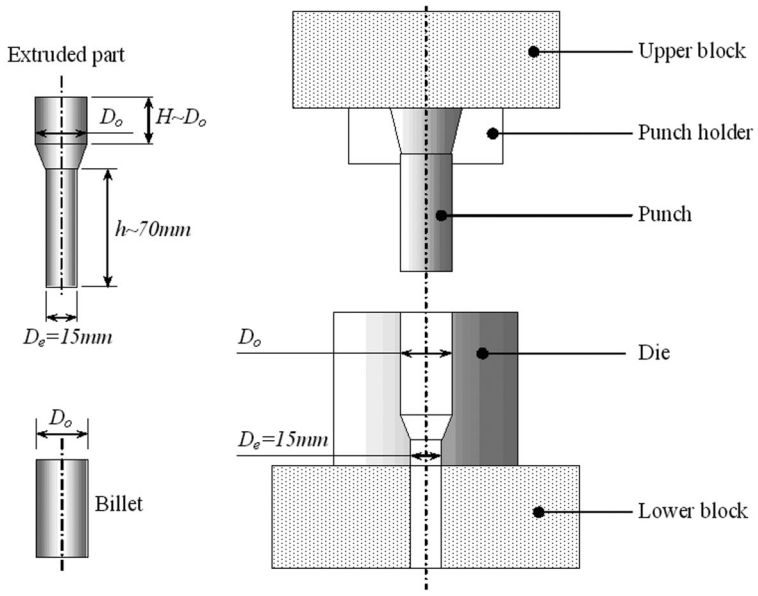

Fig. 7 Sketch for the experimental setup

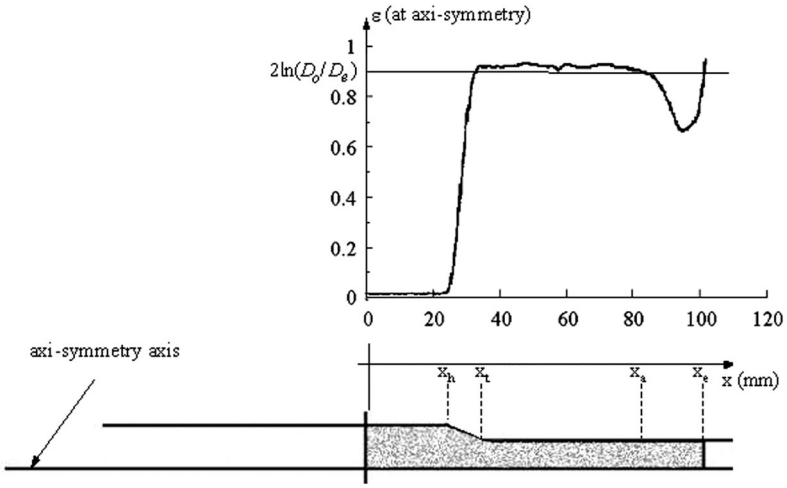

Fig. 8 Final geometry of the forward extruded part and strain distribution at its centerline

only be determined by FE modeling, and thus hardness predictions can be made based on only numerically obtained values of strain.

Results of the Extrusion Tests. The extruded parts were cut at the mid-plane and the Brinell hardness measurements ($F/D^2 = 30$) were taken at the centerline of the extruded portion. Table 5 lists the average of the measured Brinell hardness (five measurements for each extruded part), and the corresponding impression diameter. These are the average values of 20 pieces of extruded part for each strain and material. 200 pieces were extruded totally.

The analytical model was then used to determine the hardness at the centerline. Figure 9 gives a comparison between measured and predicted hardness. Although the proposed equation underestimates the hardness, the predicted trend of the change in hardness with effective strain conforms well to the experimentally determined trend. The maximum error is less than 13%, which can be considered to be satisfactory for predicting hardness distribution in cold forged parts.

Discussion

Comparisons with the data attest the accuracy of the proposed equation, even though there may be numerous sources of error. As a source of measurement errors, piling-up or sinking-in around the circumference of the impression may detract from the accuracy of optical readings. Besides, we extensively used the conversion table between Vickers and Brinell hardness. Conversion factors have limited accuracy. The behavior of the material in resisting indentation could be different for spherical and pyramidal indenters. Any inhomogeneity may cause different readings especially for Vickers hardness, which has much smaller impression than Brinell's. On the other hand, large size of Brinell's impression leads to homogenization of mechanical properties. Especially, at locations where hardness gradient is high, Brinell hardness represents average hardness around the point at which measurement is taken. Impression size to part size ratio in our experiments as indicated in Table 5 is high, which might have led to measured values higher than the actual. Besides, sometimes specimens were cut to take measurements in an interior region. During cutting operation, induced plastic deformation may increase the hardness.

The source of error may also lie in the model. Stress–strain curve of a material may not perfectly fit into a power relation as assumed in employing Eq. (2). Equality of "*m*" in Eq. (3) and "*n*" of Eq. (2) was assumed in the model. However, these expo-

Table 5 Average measured values of Brinell hardness at the centerline of the extruded parts and corresponding impression diameters

	HB (kgf/mm^2)		*d* (mm)	
Strain	C40	St37	C40	St37
0.25	205	195	4.21	4.32
0.50	230	220	3.99	4.08
0.90	250	235	3.83	3.95
1.20	260	245	3.76	3.87
1.40	265	250	3.73	3.83

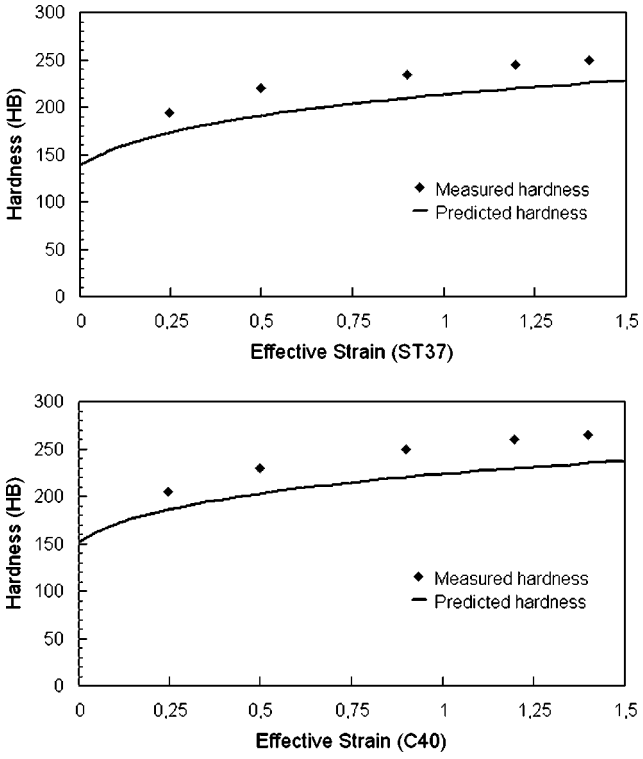

Fig. 9 Data points indicate the measured Brinell hardness (kgf/mm^2). The line shows the hardness predicted by the proposed equation (Eq. (12) and Eq. (1)).

nents do not exactly have the same values. Also, the universality of α and β in Eq. (8) and the particular values used in this study were just approximations.

Conclusions

In this study, we presented an analytical model to predict Brinell hardness distribution in cold formed products. Application of this model requires only flow curve constants (κ and n), which can be obtained through a simple compression test, and effective strain distribution, which can be obtained through a FE analysis of the cold forming process. The predictions of the model were compared with experimental data, and the accuracy of these predictions was quite satisfactory.

Acknowledgments

This paper is based on the work supported by KANCA, a cold forging company, and the Scientific Research Projects of Bogazici University with the code number 04A602. The experiments were performed in KANCA, and the hardness measurements were taken in METU and KANCA. We express our thanks to Mr. Bulent Yavuz and Professor Erman Tekkaya, METU, for taking hardness measurements.

References

[1] Kim, H., Lee, S.-M., and Altan, T., 1996, ''Prediction of Hardness Distribution in Cold Backward Extruded Cups,'' J. Mater. Process. Technol., **59**, pp. 113–121.
[2] Gouveia, B. P. P. A., Rodrigues, J. M. C., and Martins, P. A. F., 1998, ''Steady State Finite-Element Analysis of Cold Forward Extrusion,'' J. Mater. Process. Technol., **73**, pp. 281–288.
[3] Gouveia, B. P. P. A., Rodrigues, J. M. C., and Martins, P. A. F., 1998, ''Finite Element Modeling of Cold Forward Extrusion and Combined Eulerian—Lagrangian Formulations,'' J. Mater. Process. Technol., **80–81**, pp. 647–652.
[4] Ruminski, M., Luksza, J., Kusiak, J., and Packo, M., 1998, ''Analysis of the Effect of Die Shape on the Distribution of Mechanical Properties and Strain Field in the Tube Sinking Process,'' J. Mater. Process. Technol., **80–81**, pp. 683–689.
[5] Choi, Y., Park, J. H., Kim, B. M., Choi, J. C., and Min, B. H., 2000, ''Estimation of Relation between Effective Strain and Hardness by Rigid-Plastic FEM,'' Metals and Materials, **6**, pp. 111–116.
[6] Tekkaya, A. E., 2001, ''Improved Relationship between Vickers Hardness and Yield Stress for Cold Formed Materials,'' Steel Res., **72**, pp. 304–310.
[7] Boyer, H. E., 1987, Hardness Testing, ASM International, US.
[8] Tabor, D., 1996, ''Indentation Hardness: Fifty Years On, A Personal View,'' Philos. Mag. A, **74**, pp. 1207–1212.
[9] Timoshenko, S. and Goodier, J. N., 1951, *Theory of Elasticity*, McGraw–Hill.
[10] Tabor, D., 1951, *The Hardness of Metals*, Clarendon Press, New York.
[11] Tabor, D., 1948, ''A Simple Theory of Static and Dynamic Hardness,'' Proc. R. Soc. London, Ser. A, **192**, pp. 247–274.
[12] Tirupataiah, Y., and Sundararajan, G., 1991, ''On the Constraint Factor Associated With the Indentation of Work-Hardening Materials With a Spherical Ball,'' Metall. Trans. A, **22A**, pp. 2375–2384.
[13] Chaudhri, M. M., 1996, ''Subsurface Plastic Strain Distribution Around Spherical Indentations in Metals,'' Philos. Mag. A, **74**, pp. 1213–1224.
[14] Sinclair, G. B., Follansbee, P. S., and Johnson, K. L., 1985, ''Quasi-Static Normal Indentation of an Elasto-Plastic Half Space by a Rigid Sphere-II Results,'' Int. J. Solids Struct., **21**, pp. 865–888.
[15] Francis, H. A., 1976, ''Phenomenological Analysis of Plastic Spherical Indentation,'' Trans. ASME; J. Eng. Mater. Technol., **98**, pp. 272–281.
[16] Chen, W. F. and Han, D. J., 1988, *Plasticity for Structural Engineers*, Springer-Verlag, New York.
[17] Richmond, O., Morrison, H. L., and Devenpeck, M. L., 1974, ''Sphere Indentation With Application to the Brinell Hardness Test,'' Int. J. Mech. Sci., **16**, pp. 75–82.
[18] Follansbee, P. S., and Sinclair, G. B., 1984, ''Quasi-Static Normal Indentation of an Elasto-Plastic Half-Space by a Rigid Sphere-I. Analysis,'' Int. J. Solids Struct., **20**, pp. 81–91.
[19] Edlinger, M. L., Gratacos, P., Montmitonnet, P., and Felder, E., 1993, ''Finite Element Analysis of Elastoplastic Indentation with a Deformable Indenter,'' Eur. J. Mech. A/Solids, **12**, pp. 679–698.
[20] Guyot, N., Kosior, F., and Maurice, G., 2000, ''Numerical Study of the Brinell Hardness Test of Elastoplastic Indentation,'' Z. Angew. Math. Mech., **80**, pp. 555–563.
[21] Hill, R., Storakers, B., and Zdunek, A. B., 1989, ''A Theoretical Study of the Brinell Hardness Test,'' Proc. R. Soc. London, Ser. A, **423**, pp. 301–330.
[22] Biwa, S., and Storakers, B., 1995, ''An Analysis of Fully Plastic Brinell Indentation,'' J. Mech. Phys. Solids, **43**, pp. 1303–1333.
[23] Mesarovic, S., and Fleck, N. A., 1999, ''Spherical Indentation of Elastic-Plastic Solids,'' Proc. R. Soc. London, **455**, pp. 2707–2728.
[24] Chaudri, M. M., 2000, ''Strain Hardening around Spherical Indentations,'' Phys. Status Solidi A, **182**, pp. 641–652.
[25] Matthews, J. R., 1980, ''Indentation Hardness and Hot Pressing,'' Acta Metall., **28**, pp. 311–318.
[26] Taljat, B., Zacharia, T., and Kosel, F., 1998, ''New Analytical Procedure to Determine Stress-Strain Curve from Spherical Indentation Data,'' Int. J. Solids Struct., **35**, pp. 4411–4426.
[27] Tirupataiah, Y., and Sundararajan, G., 1987, ''A Comprehensive Analysis of the Static Indentation Process,'' Mater. Sci. Eng., **91**, pp. 169–180.
[28] Nayebi, A., El Abdi, R., Bartier, O., and Mauvoisin, G., 2002, ''New Procedure to Determine Steel Mechanical Properties from the Spherical Indentation Technique,'' Mech. Mater., **34**, pp. 243–254.
[29] Carlsson, S., and Larsson, P.-L., 2001, ''On the Determination of Residual Stress and Strain Fields by Sharp Indentation Testing. Part II: Experimental Investigation,'' Acta Mater., **49**, pp. 2193–2203.
[30] Dowling, N. E., 1999, *Mechanical Behavior of Materials: Engineering Methods for Deformation Fracture and Fatigue*, Prentice–Hall, NJ.
[31] Oberg, E., Jones, F. D., and Horton, H. L., 1979, *Machinery's Handbook*, 21st ed., Industrial Press Inc., New York.
[32] Pöhland, K., 1989, *Materials Testing for the Metal Forming Industry*, Springer-Verlag, Berlin.
[33] Demir, A., 2001, ''Prediction of Brinell Hardness Distribution in Cold Formed Parts,'' Bogazici University, MS thesis, Istanbul.